

Assessing the Function of Motor Cortex: Single-Neuron Models of How Neural Response Is Modulated by Limb Biomechanics

Robert Ajemian,^{1,*} Andrea Green,² Daniel Bullock,^{3,4} Lauren Sergio,⁵ John Kalaska,^{2,*} and Stephen Grossberg^{3,4}

¹McGovern Institute for Brain Research, Massachusetts Institute of Technology, Cambridge, MA 02139, USA

²Groupe de recherche sur le système nerveux central (FRSQ), Département de physiologie, Université de Montréal, QC H3C 3J7, Canada

³Department of Cognitive and Neural Systems, Boston University, Boston, MA 02215, USA

⁴Center of Excellence for Learning in Education, Science, and Technology, Boston, MA 02215, USA

⁵School of Kinesiology and Health Science, York University, Toronto, ON ON M3J 1P3, Canada

*Correspondence: ajemian@mit.edu (R.A.), kalaskaj@physio.umontreal.ca (J.K.)

DOI 10.1016/j.neuron.2008.02.033

SUMMARY

Do neurons in primary motor cortex encode the generative details of motor behavior, such as individual muscle activities, or do they encode high-level movement attributes? Resolving this question has proven difficult, in large part because of the sizeable uncertainty inherent in estimating or measuring the joint torques and muscle forces that underlie movements made by biological limbs. We circumvented this difficulty by considering single-neuron responses in an isometric task, where joint torques and muscle forces can be straightforwardly computed from limb geometry. The response for each neuron was modeled as a linear function of a “preferred” joint torque vector, and this model was fit to individual neural responses across variations in limb posture. The resulting goodness of fit suggests that neurons in motor cortex do encode the kinetics of motor behavior and that the neural response properties of “preferred direction” and “gain” are dual components of a unitary response vector.

INTRODUCTION

The question of whether the activity of neurons in primary motor cortex (M1) signals specific muscular details causal to movement or, instead, high-level motor commands has been central to the study of M1 function ever since the advent of experimental neurophysiology over a century ago. Fritsch and Hitzig’s discovery in 1870 of a motor cortex that, when electrically stimulated, evoked twitches in a small group of related muscles was challenged (in its interpretative details) three years later by Ferrier’s experiments, in which electrical stimulation of motor cortex was suggested to evoke components of natural behaviors (Phillips, 1975; Taylor and Gross, 2003). The first direct recording evidence that the activity of individual neurons in M1 is often better correlated with the causal mechanisms underlying motor behavior (muscle force or activation) than with an overt kinematic de-

scription of the behavior itself (joint angle position) was obtained through the single-joint neurophysiological studies of Evarts (1968, 1969). Nevertheless, other single-joint studies indicated that some M1 activity was related to noncausal motor output parameters, such as the current joint angle and the direction of the next movement in a repeated sequence (Thach, 1978). When the domain of neurophysiological inquiry expanded to the study of multijoint reaching movements (Georgopoulos et al., 1982), the converse notion gained further credence: M1 activity may indeed reflect the encoding of high-level parameters of motor behavior, such as end-effector velocity or position, rather than the generative details of movement. Indeed, most current brain-machine interfaces for the control of robotic devices are designed to extract signals about the kinematics of motor output intentions from the activity of populations of motor cortex neurons (Wessberg et al., 2000; Serruya et al., 2002; Taylor et al., 2002).

This question of what parameters are encoded in M1—often expressed as the simplistic dichotomy of “muscles or movements”—continues to cause considerable controversy to this day (Loeb et al., 1996; Georgopoulos, 1995; Scott, 2000). A major source of the contention lies in the difficulty of knowing how the activity of M1 neurons “should” look. In particular, if M1 activity is assumed to encode muscle forces or joint torques, then accurate estimates or measurements of those forces or torques, as they vary in time, are required to establish this correlation. In the case of single-joint motions, this requirement does not pose significant difficulty: the relationship between kinematics (i.e., joint angle) and the underlying causal dynamics (joint torque and muscle forces) is straightforward, and thus can be directly measured or imputed. However, as soon as movements with two degrees of freedom (DOF) are considered, it becomes difficult to accurately estimate or measure muscle forces and joint torques (Zajac, 1989), and these problems are amplified for movements with more than two DOFs.

Thus, steep onset of the “curse of dimensionality” complicates the modeling of movement dynamics. This circumstance, in turn, confounds efforts to establish strong correlations between movement dynamics and the responses of neurons in M1. As an alternative to estimating or measuring movement dynamics, studies have correlated neural activity with EMG activity (a proxy of muscle activation signals), but the high noise level and

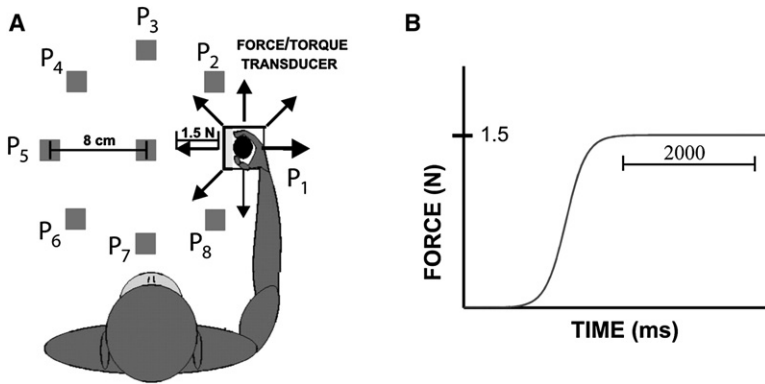


Figure 1. Experimental Protocol

(A) An isometric center-out task is performed in the horizontal plane at the nine different workspace locations placed in a circle (of radius of 8 cm) surrounding a central workspace location.

(B) A constant force level of 1.5 N must be generated and maintained for 2000 ms in the appropriate direction.

poor temporal resolution of EMG measurements complicate these efforts.

In this paper, the problem of accurately modeling movement dynamics is circumvented for a four-DOF arm by considering an isometric task. While isometric tasks are only a subset of a wider repertoire of motor behaviors, the computations of joint torques, muscle forces, and muscle activations are rendered tractable. As a result of this tractability, hypotheses about the correlations between cell activity and variables related to biomechanical force generation can be tested at a level of rigor previously unattainable. Specifically, it is demonstrated that parameters of biomechanical force generation can be mapped to *individual* neurons in M1 (as opposed to populations of such neurons). These fits explain a significant amount of response variability at the single-cell level, and thus support the hypothesis that M1 controls force output. Finally, the single-neuron approach unifies our understanding of tuning curve parameters: whereas a cell's preferred direction and gain were previously considered independent response components, they are shown to be dual manifestations of a unitary response vector.

Background

In the multijoint control of the primate upper limb, neurons in motor cortex are tuned to the direction of movement in center-out movement tasks (Georgopoulos et al., 1982; Schwartz et al., 1988) and to the direction of force exertion in center-out isometric tasks (Georgopoulos et al., 1992; Taira et al., 1996). The canonical description of a cell tuning curve is

$$\nu(\omega) = b_0 + b_1 \cos(\omega - \omega_{PD}) \quad (1)$$

where ν is a cell's activity as a function of ω , the movement (or force) direction of the hand; b_0 is the cell's baseline level of activity; b_1 is the depth of modulation or gain of the cell's tuning curve; and ω_{PD} is the preferred direction of the cell or the direction of movement (or force) that elicits the maximal cell response.

Of the four parameters on the right-hand side of Equation 1, three are intrinsic to the cell: b_0 , b_1 , and ω_{PD} . Each of these intrinsic parameters has been shown to vary as a function of behavioral context (Georgopoulos et al., 1984; Kalaska and Hyde, 1985; Kettner et al., 1988; Kalaska et al., 1989; Caminiti et al., 1990; Lacquaniti et al., 1995; Scott and Kalaska, 1997; Sergio and Kalaska, 1997, 1998, 2003; Sergio et al., 2005; Kakei et al.,

1999, 2003; Gandolfo et al., 2000; Cabel et al., 2001; Padoa-Schioppa et al., 2001; Kurtzer et al., 2005). The parameter ω_{PD} has been the most heavily investigated, because it is the one direct determinant of cell response as a function of a task variable (movement direction or the direction of force exertion). Less is known about a cell's gain, which is defined as b_1 . Because b_1 is not an angular measure, it does not indicate a directional preference in and of itself; nonetheless, as the gain (or amplitude) of a tuning curve, it does signify the strength with which a directional preference is instantiated during a particular task context.

RESULTS

The data in this paper are taken from a neurophysiological experiment in which nonhuman primates performed an isometric task from nine different hand positions (see Figure 1). A short description of the paradigm is provided in the [Experimental Procedures](#); more detailed descriptions can be found in [Sergio and Kalaska \(1997, 2003\)](#). During the task, cell recordings were taken from the caudal part of M1, with most neurons recorded from that part of M1 located in the rostral bank of the central sulcus. From these recordings, distinct tuning curves were assessed for task-related cells at *each* of the nine positions, for a total of nine tuning curves per cell. Note that cell activity was averaged, for the purposes of this study, over a 2000 ms target-hold epoch, during which time the hand maintained a state of static force equilibrium with the manipulandum handle. Note also that each different location where the hand was positioned corresponds to a particular arm posture. The joint angles for these arm postures were recorded and are presented in [Table 1](#).

The model of cell recruitment makes only one assumption: cells are active within the task according to the rule

$$\nu(\vec{\tau}_a) = [b_0 + \vec{\tau}_a \bullet \vec{\tau}_{PD}]^+ \quad (2)$$

where $\vec{\tau}_a$ denotes the torque applied by the whole arm during the task, $\vec{\tau}_{PD}$ denotes a cell's preferred vector of torque application, ν and b_0 remain as defined in Equation 1, " \bullet " denotes a dot product, and $[\]^+$ denotes positive rectification. $\vec{\tau}_{PD}$ is a vector parameter intrinsic to the cell that defines the direction in joint torque space to which the cell responds maximally. It is $\vec{\tau}_{PD}$, then, which fully defines the response of a model cell beyond its baseline discharge level. Joint torque space is here 4-dimensional (4D), since an arm model with four DOF is used (see [Experimental Procedures](#)). The dot product formulation generalizes upon the original cosine formulation of cell tuning by merging the direction and amplitude components of tuned response into a unitary vectorial

Table 1. Joint Angles and Hand Locations at the Nine Different Postures

Hand Location	Joint Angles (Deg.)				Hand Coordinates (cm)		
	θ_1	θ_2	θ_3	ϕ	x	y	z
P ₀	-16	-15	-12	104	14.0	-1.0	15
P ₁	6	-1	-11	82	19.7	-3.3	15
P ₂	22	4	-27	64	22.0	-9.0	15
P ₃	19	17	-31	59	19.7	-14.7	15
P ₄	-1	21	-37	73	14.0	-17.0	15
P ₅	-18	5	-47	95	8.3	-14.7	15
P ₆	-32	-13	-40	113	6.0	-9.0	15
P ₇	-37	-13	-17	117	8.3	-3.3	15
P ₈	-11	6	-25	95	14.0	-9.0	15

There are three degrees of freedom at the shoulder: flexion/extension, abduction/adduction, and internal/external rotation. There is only one degree of freedom at the elbow: flexion/extension. The precise geometry of the arm model is provided in the [Experimental Procedures](#). Note the relatively modest angular excursions (<60°) for all four angles, particularly shoulder abduction/adduction and internal/external rotation. The Cartesian coordinate system for representing hand location is centered at the right shoulder, with the x axis pointing away from the body, the y axis pointing across the body to the right, and the z axis pointing into the ground.

description (Mussa-Ivaldi, 1988; Zhang and Sejnowski, 1999; Ajemian et al., 2001). It is shown later that if certain modest assumptions are made, a dot product model in joint torques is equivalent, for the case of an isometric task, to a dot product model of muscle forces or muscle activations. Therefore, the results apply broadly to any of a class of models that emphasizes musculoskeletal kinetics in interpreting motor cortical output.

Given Equation 2 and the data on arm postures, tuning curves can be simulated across the workspace for any model cell. The key step is realizing that in an isometric task, the applied static force at the hand can be related to the torque of the whole arm through

$$\vec{\tau}_a = \mathbf{J}^T(\theta)F_h \quad (3)$$

where $\mathbf{J}^T(\theta)$ denotes the transpose Jacobian of the kinematic relationship between joint angles and end-effector position evaluated at posture θ , F_h denotes the static force applied by the hand, and $\vec{\tau}_a$ denotes the whole arm torque. Under certain assumptions, this mapping is unique (see [Experimental Procedures](#) for details), and thus, the applied torque is computable.

Population-Level Analyses: PD shifts, Gain Changes, and Model Geometry

For the population-level analyses, an additional assumption is made. The distribution of $\vec{\tau}_{PD}$ across a population of cells in motor cortex is assumed to be *uniform* in joint torque space. As will be shown, this assumption, too, can be relaxed considerably without affecting the results of the paper. It is chosen for the sake of specificity, since a specific distribution is required to define a population of cells over which response property changes can be tabulated. For analyses focusing on PD shifts and gain changes, b_0 can assume any value because it automatically drops out of the analyses. Thus, these population statistics are

generated with zero free parameters, and the model illustrates response property changes that can be expected wholly on the basis of biomechanical considerations.

Shifts in Preferred Directions

If cells were encoding endpoint force in a Cartesian spatial coordinate system, a cell’s preferred direction would, by definition, be predicted to remain invariant across postures. However, in agreement with numerous other studies, Sergio and Kalaska (1997, 2003) consistently showed statistically significant changes in preferred directions across the workspace. A cell’s “PD shift” at one of the eight peripheral workspace locations was defined as its rotation with respect to the cell’s PD at the central location. With this convention, a population-level analysis revealed “a significant difference in the distribution of PD shifts across the eight peripheral postures” (Sergio and Kalaska, 2003). Figure 2A plots the data on PD shifts for a population of cells (see [Experimental Procedures](#) for details). The distribution of PD shifts exhibits a distinct pattern whereby cells tend to show counterclockwise PD shifts at the leftward locations and clockwise shifts at the rightward locations. The model comparison is plotted on the right half of Figure 2A. The model clearly captures the basic trends in the distribution of PD shifts. For example, clockwise shifts dominate at the leftward locations both in the data (81.5%, 77.8%, and 65.4%) and in the model (75.9%, 79.1%, and 64.3%).

Gain Changes

Sergio and Kalaska (2003) also showed that cells change their gain across the workspace. The gain change for a cell at a peripheral location is defined with respect to the cell’s gain at the central location using a measure called the dynamic range (DR) ratio. While the vast majority of individual cells exhibited statistically significant gain changes at multiple workspace locations, “there was no systematic difference in the distributions of DR ratios as a function of hand location (ANOVA, $P > 0.01$).” Thus, if there are systematic spatial biases in a cell’s gain value, the effects are small in comparison with PD shifts. Nonetheless, it makes sense to examine whether the proposed model can identify any sub-threshold trends in the gain change data, because the model reproduces PD shifts fairly well and because the model treats PD shifts and gain changes as dual manifestations of a single response vector that determines cell activity across all conditions.

Figure 2B plots the distribution of gain changes across the workspace for the data and the model. A fractional gain change (which is simpler than the DR ratio) is used to quantify these changes:

$$\Delta b_i^j = \frac{b_i^j - b_1^c}{b_1^c}$$

where b_i^j denotes the cell’s gain at location i , and b_1^c denotes the cell’s gain at the central location. Note that this definition results in a normalized measure of gain change that ignores the cell’s absolute gain values and takes into consideration only the gain ratio between the central and peripheral locations. A clear trend is seen in the simulations, whereby a majority of model cells show gain decreases when the hand is situated closer to the shoulder (locations P₇, P₈, and P₁ in Figure 1). At workspace locations further away (P₂, P₃, and P₄), a majority of cells show

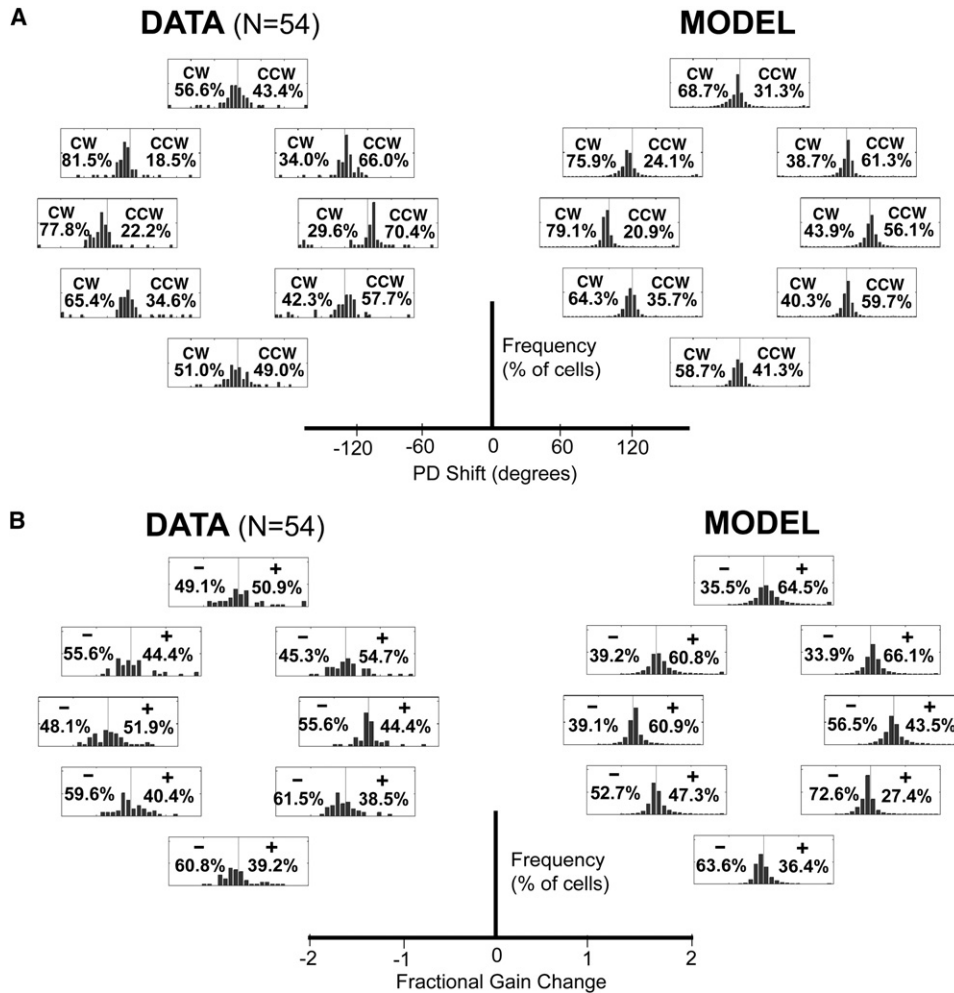


Figure 2. Response Property Changes across the Workspace

(A) PD shifts for data and model. The location of each histogram within a circle of histograms corresponds to the workspace location of the hand at which the isometric task is performed. The x axis of each histogram corresponds to the shift in a cell's PD, at the corresponding posture, with respect to the cell's PD at the center workspace location. Positive shifts are counterclockwise (CCW) and negative shifts are clockwise (CW). The bins are each 10°.

(B) Gain changes across the workspace for data and model. The location of each histogram within a circle of histograms again corresponds to the workspace location of the hand at which the isometric task is performed. The x axis of each histogram corresponds to a cell's change in gain at the corresponding posture with respect to the cell's gain at the center workspace location (see text for definition of gain change). Positive changes signify gain increases. Bin width is 0.15.

gain increases. This same tendency for gain decrease is seen in the data at the lower postures, although the data do not show a pronounced tendency for gain increase at the upper postures.

Model Geometry

The model describes cell recruitment as a dot product or vector projection that takes place in joint torque space. The task, however, employs an invariant sampling regimen that is uniform in Cartesian force space (as opposed to joint torque space). Therefore, insight into how the model explains response property variation follows from an analysis of how the transpose Jacobian, $J^T(\theta)$, converts a uniform sample of Cartesian forces into a non-uniform sample of joint torques in a posture-dependent fashion.

Figure 3 illustrates the general properties of transforming by the transpose Jacobian. The uniform or circular sampling in 2D Cartesian force space is converted into a skewed or elliptical sampling in a 2D subspace of the 4D joint torque space. The ma-

nor and minor axes of the torque ellipse, denoted by the red vectors, define a basis for the particular 2D subspace in joint torque space to which Cartesian force vectors are mapped at that posture. The ratio of the magnitudes of these axes quantifies the degree of skewing of the transformation.

At a given posture, a cell's preferred direction arises from the relative orientation of the three vectors \vec{r}_{PD} , \vec{r}_{MAJOR} , and \vec{r}_{MINOR} . A cell's gain arises from the magnitude of the projection of \vec{r}_{PD} onto the subspace spanned by \vec{r}_{MAJOR} and \vec{r}_{MINOR} . While \vec{r}_{PD} remains, by assumption, invariant (in joint torque space) across postures, \vec{r}_{MAJOR} and \vec{r}_{MINOR} vary across postures because they are derived from the transpose Jacobian, which itself changes in a posture-dependent fashion. Therefore, PD shifts and gain changes observed in cell activity when it is plotted in a 2D Cartesian force space arise explicitly from the well-defined global geometry of the transformation between joint torques and endpoint

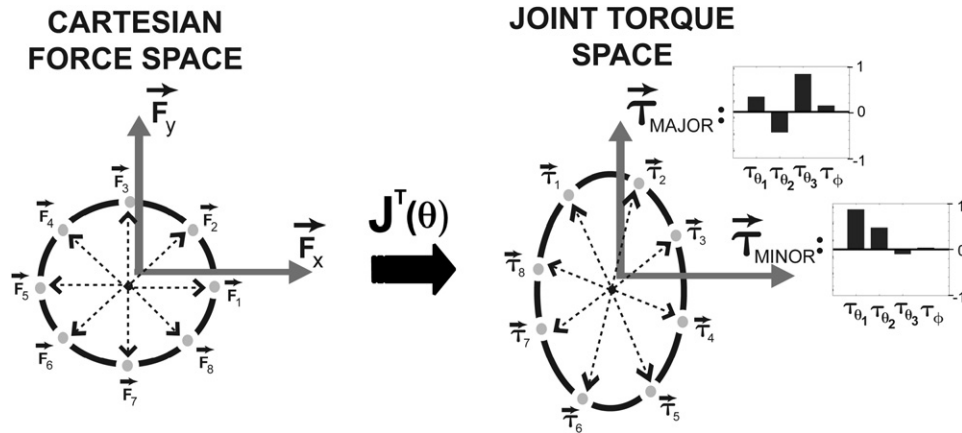


Figure 3. Transformation of Cartesian Forces into Joint Torques at the Center Workspace Location

The uniform sampling regimen in the isometric center-out task is converted into a skewed distribution of joint torques contained within a 2D subspace of the 4D joint torque space. The major and minor axes of the torque ellipse constitute a basis set for the 2D subspace. Unit vectors in the directions of these axes are denoted by the corresponding bar graphs: each bar corresponds to the magnitude of the torque contribution along a particular degree of freedom. $\tau_{\theta 1}$ corresponds to the shoulder torque in the flexion/extension dimension; $\tau_{\theta 2}$ corresponds to the shoulder torque in the abduction/adduction dimension; $\tau_{\theta 3}$ corresponds to the shoulder torque in the internal rotation/external rotation dimension; and τ_{ϕ} corresponds to the elbow torque. See [Experimental Procedures](#) for details.

forces. [Figure 4](#) depicts posture-dependent changes in $\mathbf{J}^T(\theta)$ by plotting the joint torque ellipses that arise at each posture.

Single-Cell Analysis: Model Verification, Generalization, and Consistency

Many models of neural activity in motor cortex have been developed based on the assumption that cell response reflects movement biomechanics (Mussa-Ivaldi, 1988; Bullock and Grossberg, 1988; Sanger, 1994; Tanaka, 1994; Scott and Kalaska, 1997; Bullock et al., 1998; Ajemian et al., 2000; Todorov, 2000; Scott et al., 2001; Baraduc et al., 2001; Trainin et al., 2007), and these models have been used to explain a variety of experimental findings. However, a major drawback to all of these models is that their predictions can only be compared to data at the population level, either in the form of population statistics or aggregate population response. In the case of population statistics, a typical finding is as follows: $x\%$ of cells are well-correlated with variable A in the data; $y\%$ of cells are well-correlated with variable A in the model; x approximates y . In the case of aggregate population response, a neural population vector is constructed and shown to approximate the vectorial representation of a movement variable (such as force or velocity).

Thus, these models, while envisioned at the level of single cells, nonetheless lack single-cell resolution, because parameters of the model cannot be mapped onto individual cells in the data. As a result, the models can be shown to be generally consistent with data at the population level, but they cannot be falsified by data at the stricter single-cell level. It is entirely possible that a model correctly describes the data at the population level, but fails to correctly predict how any *given* cell should respond in a particular task. For example, our model correctly reproduces the dominant trends in PD shifts and gain changes at the level of population statistics ([Figure 2](#)), but it may not correctly predict the response profile of any individually chosen neuron.

In the analyses that follow, our model is tested at the single-cell level by individually mapping the four parameters of the

model to each of 54 cells. Specifically, a cell is fully described in the model by its preferred torque vector:

$$\vec{\tau}_{PD}^i \equiv \left\langle \begin{matrix} \delta\theta_1^i \\ \delta\theta_2^i \\ \delta\theta_3^i \\ \delta\phi^i \end{matrix} \right\rangle$$

where the superscript i denotes the specific cell from the database; $\delta\theta_1^i$, $\delta\theta_2^i$, and $\delta\theta_3^i$ correspond to the three shoulder components of the preferred joint torque vector (see [Experimental Procedures](#) for definition of shoulder DOF); and $\delta\phi^i$ corresponds to the elbow component of the preferred torque vector. Once these four parameters have been determined, the cell's response profile is also determined. [Figure 5](#) shows an example of a specific preferred torque vector and the resulting cell response profile.

For each cell, there are 17 data points that constitute its response profile: 9 different preferred directions (one at each posture) and 8 different gain changes (the change in gain relative to baseline at the eight peripheral postures). Therefore, the power of the model to fit data at the single-cell level can be systematically assessed by seeing how well the four model parameters can explain the 17 data points on a neuron-by-neuron basis. Here it should be noted that only three of the model parameters are actually free parameters. This is because the model predicts the changes in gain and not the absolute values of gain. Thus, preferred torque vectors are all considered to have a fixed magnitude of unity across cells, and once three model parameters are specified, the fourth is automatically determined (see [Experimental Procedures](#) for details). Below are two methods of fitting the three free parameters of the model to the 17 data points of the response profile on a neuron-by-neuron basis.

Model Verification

In this section, two of the three free parameters will be used to fit a cell's preferred direction at the central posture. Thus, by

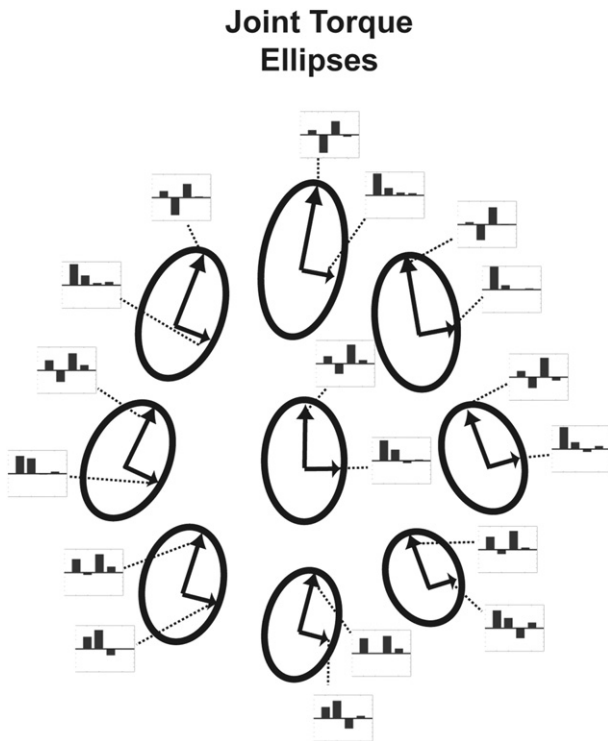


Figure 4. Posture-Dependent Variations in the Effect of the Transpose Jacobian as Shown through Torque Ellipses

The location of each torque ellipse corresponds to the location in the workspace where the center-out isometric task was performed. The bar graphs depict unit vectors in joint torque space corresponding to the major and minor axes of the torque ellipse. The tilt of the ellipses corresponds to the net clockwise or counterclockwise rotation of PDs across the entire sample of cells. Note how the skewing of the torque ellipses is more severe at the outer workspace locations. Note also how the major and minor axes vary significantly across the workspace. It is the hard-to-visualize geometry of these changes in 4D joint torque space that give rise to the observed rotation of a cell's PD.

design, the model-preferred direction at the central posture exactly matches the actual preferred direction at the central posture (because a single preferred direction requires two model parameters for specification, and two model parameters are devoted to that fit). The lone remaining free parameter is used to fit all eight instances of gain change, and Figure 6A plots all 426 instances of predicted gain change versus actual gain change across the 54 cells (see Experimental Procedures). As can be seen, with a single parameter per cell, the model does a good job of capturing the gain changes across the entire spectrum of gain variation from decreases of 50% to increases of 250%. The resulting regression line is

$$y = 0.96x - 0.01$$

where the 95% confidence intervals about the slope and y-intercept are, respectively, [0.88 1.03] and [-0.04 0.03]. Thus, this regression line very closely approximates the desired line of $y = x$ (shown in the Figures 6A and 6B as the dashed line), in which case the model gain, by itself, predicts the actual gain. Moreover, the R^2 statistic for the model is 0.60, meaning that

with a single parameter per cell, the model accounts for 60% of the variation in all 426 instances of gain change.

Model Generalization

The success of any model depends critically on its ability to generalize: a model must be shown to explain data outside of the context in which it is formulated. Mathematically, this means that if model parameters are fit to data in one context, those same parameters should apply successfully to data generated in a novel context. Population-level models (Mussa-Ivaldi, 1988; Scott and Kalaska, 1997; Bullock et al., 1998; Ajemian et al., 2000; Todorov, 2000; Scott et al., 2001; Trainin et al., 2007) are incapable of meaningful generalization, because even when the population-level analyses agree across contexts, it is impossible to tell if any individual cell showed the predicted context-dependent behavior with a *fixed* set of parameters.

Our model assumes a unification of a cell's preferred direction and its gain. Therefore, if the model parameters are fit to one of these response properties, the model should also apply successfully to the other response property. To that end, for each of the 54 cells, we chose three free model parameters to best fit a cell's eight measured gain changes (see Experimental Procedures). None of the model parameters were devoted to explaining any of a cell's nine preferred directions. Yet, if the model's proposed relationship between gain and preferred direction is correct, the model should be able to predict the preferred directions with some success. Figures 6B–6D show the results. In Figure 6B, all 426 instances of gain change across the 54 cells are plotted. With three parameters per cell devoted to capturing gain changes, the resulting fit is extremely good. The regression line is

$$y = 1.04x$$

where the 95% confidence intervals about the slope and y-intercept are, respectively, [0.99 1.09] and [-0.04 0.01]. Moreover, the R^2 statistic for the model is 0.77, meaning that with three parameters per cell, 77% of the variation in gain is captured.

With none of the model's parameters devoted to fitting a cell's preferred direction, the model's ability to generalize can be assessed by seeing how well the preferred directions are subsequently predicted. The median absolute difference between the actual and predicted PD values is 38.5° (mean 47.7°). Since angle is a periodic variable (and the angular difference is bounded at 180°), conventional linear regression cannot be used to judge the statistical significance of this fit. However, there is an analogous correlation measure for circular statistics (see Experimental Procedures), and the circular correlation coefficient is 0.27, which, for a sample size of 480, is statistically significant at $p < 0.001$.

Bootstrapping methods can also be used to illustrate the statistical significance of the model's PD predictions. Figure 6C plots a histogram of differences between the actual PD values and the model PD values. This histogram can be compared with a histogram of "random" differences (Figure 6D) that is constructed by sampling, with replacement, two random PD values from the pool of 480 PD values (see Experimental Procedures). Notice that the histogram in Figure 6C is centered about 0° , while the histogram of Figure 6D is relatively uniform, or even slightly

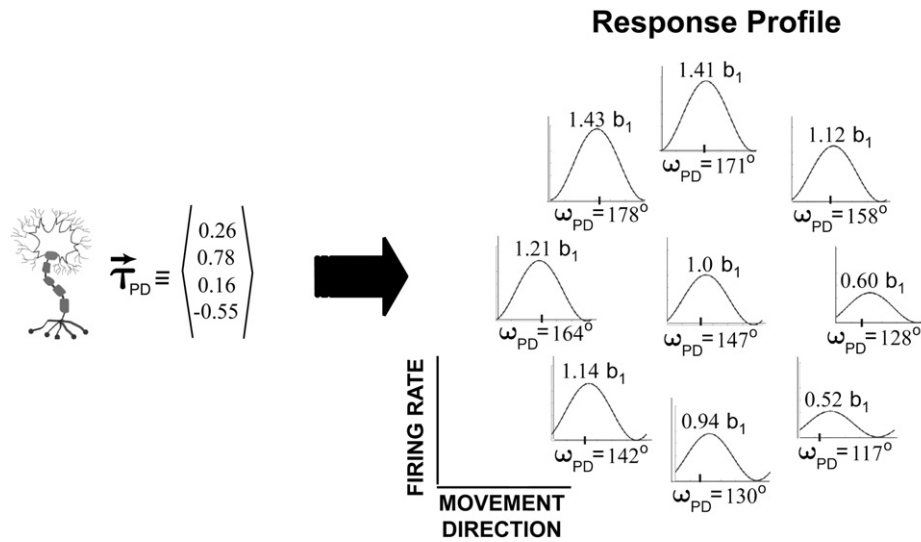


Figure 5. Response Profile for a Specific Preferred Torque Vector

The preferred torque vector is shown at the left of the figure. It consists mostly of shoulder adduction and elbow extension. Such a mechanical action would be consistent with activation of the *Triceps brachii*. However, preferred torque vectors in the model do not have to correspond to individual muscles. Rather, they correspond to the aggregate biomechanical effect of the muscle field of an output neuron in motor cortex. At the right of the figure are the resultant tuning curves at each of the nine locations. Note that the gain, according to the model, can only be assessed as a multiple of the gain b_1 at the central posture. Also note that the baseline activity level b_0 is not a part of the model and so is not explicitly highlighted in the figure.

bimodal. The median absolute difference between the randomly sampled PD values is 88.5° (mean 89.0°), which is very close to the median and mean of a uniform random distribution of angular differences (90.0°).

Model Consistency

Model parameters have been mapped to individual cells using two different methods. If the model has merit, there should be some consistency in the results obtained. Table A1 at the end of the Appendix lists the model parameters—that is, the components of $\vec{\tau}_{PD}$ —as they were mapped to each individual cell for each method. A correlation measure between the two tabulated preferred torque vectors is provided in the far right column. Since the vectors are already normalized, the correlation measure is simply the dot product. For the most part, the model's computation of a preferred torque vector is consistent across the two fitting methods. Using bootstrap techniques, the mean correlation between two randomly generated unit vectors is 0; the 95th percentile of the rank-ordered distribution is 0.81 (see Experimental Procedures). Only for four cells does the model generate a correlation coefficient of less than 0, while for over 50% of the cells (29/54), the correlation coefficient exceeded the chance level of 0.81. Given the noise in the data and joint space redundancy, it is not surprising that some cells show a slight discrepancy depending on the method of fit.

The Encoding of Muscle Force or Muscle Activation

The model, as embodied by Equation 2, formulates cell activity as resulting from the dot product of an applied torque vector and a preferred torque vector. But one could just as easily—and perhaps more naturally—conceive of cell activity as reflecting the applied muscle force vector or the corresponding

muscle activation vector (Fetz et al., 1989; Morrow and Miller, 2003):

$$v(\vec{\mathbf{M}}_a) = [b_0 + \vec{\mathbf{M}}_a \cdot \vec{\mathbf{M}}_{PD}]^+ \quad (4)$$

where $\vec{\mathbf{M}}_a$ is the applied muscle force vector and $\vec{\mathbf{M}}_{PD}$ is the preferred muscle force vector. How would the current results on PD shifts and gain changes be impacted by this reformulation?

In order to answer this question, consider the relationship between joint torques and muscle forces:

$$\vec{\tau}_a = \mathbf{J}_M^T(\theta) \vec{\mathbf{M}}_a \quad (5)$$

where $\mathbf{J}_M(\theta)$ is the vector derivative of the muscle lengths written as a function of joint angles; it is also known as the matrix of moment arms. Because of motor redundancy, it is generally not possible to invert this matrix to convert joint torques into muscle forces. However, this matrix can be inverted if a criterion is stipulated as a means of resolving the redundancy. For our purposes, the exact criterion is irrelevant; what matters is that some criterion exists and that this criterion remains similar across the workspace. Under this assumption, the matrix can be inverted by choosing the specific inverse that fulfills the criterion:

$$\vec{\mathbf{M}}_a = \mathbf{J}_M^T(\theta)^{-1} \vec{\tau}_a. \quad (6)$$

With Equations 4 and 6, it is demonstrated in the Appendix that a recruitment rule based on either muscle forces or muscle activations would produce results on PD shifts and gain changes at the population level that are the same as those based on joint torques. Therefore, these results apply to a broad class of models that are based on musculoskeletal mechanics, as opposed to end-effector forces.

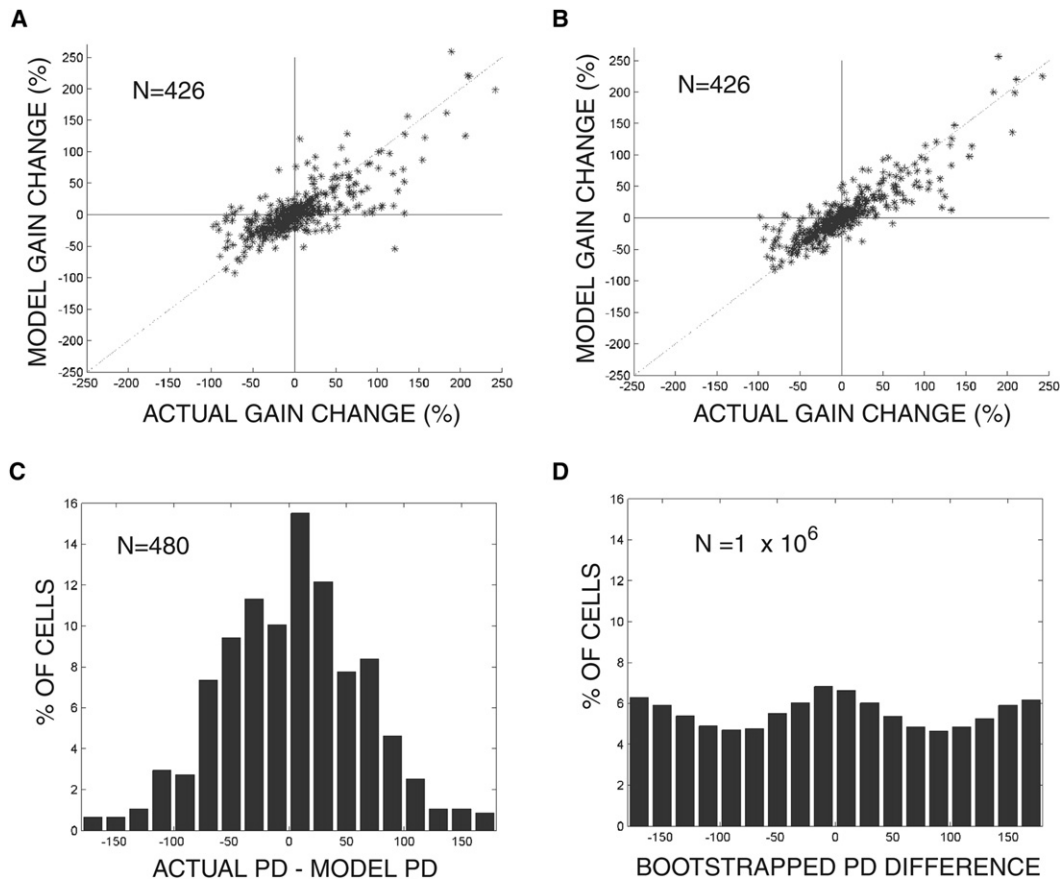


Figure 6. The Model's Ability to Fit the Data at the Single-Cell Level

(A) The results of a fit in which two free parameters are devoted to exactly fitting the cell's PD at the central posture. The remaining free parameter is used to fit the gain changes as well as possible, and the actual gain changes are plotted versus the model gain changes.

(B–D) The results of a fit in which all three free model parameters are devoted to fitting the gain changes as well as possible. (B) The actual gain changes plotted versus model gain changes. (C and D) The generalization capacity of the model in predicting a cell's nine PD values; (C) plots a histogram of differences of actual and model PD values (note how it is centered on 0), while (D) plots a histogram of bootstrapped differences between two randomly sampled PD values from the data. Note how the distribution is relatively uniform, or even modestly bimodal.

DISCUSSION

Summary of Results

The first finding of this paper is that a joint torque model of cell recruitment describes quite well the variation in response properties across a population of neurons in M1 during the performance of a multijoint isometric task. The second (and more important) finding is that the joint torque model can be tested at the resolution of single cells, a level of resolution that, to our knowledge, has not been attained previously. For the most part, the joint torque model holds up well to the increased level of scrutiny, explaining a significant amount of the changes in gain and preferred direction with only three free parameters per cell.

The issue of what parameters of motor output are encoded in M1 — often expressed by the simplistic dichotomy between muscles or movements — has been the subject of intense debate for over a century (Phillips, 1975; Taylor and Gross, 2003). Experiments were initially conducted through gross electrical stimulation of the cortex (Fritsch and Hitzig, 1870; Ferrier, 1873). This

coarse approach has evolved into single-cell recording studies in which neural firing rates are correlated with measured movement variables during stereotyped behaviors (Evars, 1968; Georgopoulos et al., 1982). Biomechanical models of the skeletomusculature have subsequently been developed and refined to more rigorously assess the adequacy of hypothesized neural correlations at the level of population statistics (Mussa-Ivaldi, 1988; Scott and Kalaska, 1997; Ajemian et al., 2000; Todorov, 2000; Trainin et al., 2007). This paper contributes to the debate by suggesting that models need to be formulated and tested at the same single-cell level at which data is collected: model parameters must be mapped onto individual cells for the dual purposes of model verification and model generalization. Only in this manner will it be possible to more thoroughly resolve matters of neural representation, whether the brain region in question is M1, nonprimary motor cortex, or other movement-related brain structures.

This model captures (1) the aggregate changes in the preferred directions and gains of the directional tuning functions of

a sample M1 neural population, and (2) the coupled changes in PD and gain of individual M1 neurons as a function of the changes in joint torques when generating static isometric forces in different arm postures. Despite this success, it would be incorrect to interpret these results as evidence that M1 neurons explicitly encode a Newtonian mechanical parameter, joint torque, especially when that parameter is closely linked to biologically based parameters such as muscle force or muscle activation. The success of the model does indicate, however, that the activity of the M1 neurons appears well-correlated to the causal kinetics and intrinsic musculoskeletal biomechanics of static isometric force output. The results also argue that the preferred direction and gain of the directional tuning function of a neuron in a particular behavioral context are not independent properties of the motor output function of an individual M1 neuron that are acquired empirically by some adaptive process. Instead, they appear to be causally linked and determined by musculoskeletal biomechanics.

These conclusions of the present single-neuron modeling effort are consistent with evidence from more standard neurophysiological manipulations that M1 activity encodes information closely related to aspects of the casual kinetics of whole-arm motor output in a variety of task conditions (Kalaska et al., 1989; Taira et al., 1996; Gribble and Scott, 2002; Sergio and Kalaska, 2003; Sergio et al., 2005; Herter et al., 2007). However, this conclusion applies primarily to the caudal part of M1, from which most of the neurons in the majority of those studies were recorded, and which also contains the greatest concentration of corticomotoneurons with monosynaptic connections with spinal alpha motoneurons (Rathelot and Strick, 2006). Neurons in the rostral part of M1 display response properties that are clearly transitional between those of the caudal M1 and those of premotor cortex neurons (Crammond and Kalaska, 1996, 2000; Cisek and Kalaska, 2005).

Finally, it is important to emphasize that the results of this modeling study are limited to the relation of M1 activity to static isometric forces. Further developments of the model would be necessary to attempt to extend it to the behavioral context of dynamic (i.e., time-varying) isometric forces and especially to the causal dynamics of arm movement.

What It Means for the Model to 'Fit' Response Property Variations

With a single parameter per cell, the model fits 60% of the variation in gain. With three parameters per cell, the model fits 77% of the variation in gain. The model also exhibits some generalization capacity in predicting a cell's PD values. Overall our model has three free parameters. How good is its overall performance compared to rival models? Unfortunately, it is difficult to say, because the only other model that has been mathematically specified is the Cartesian force-encoding hypothesis, which predicts *no* changes in a cell's gain or PD (although this model requires only one free parameter per cell, i.e., angle). Thus, our results imply one of two possibilities: (1) the model performance supports the hypothesis that many M1 neurons encode joint torques (closely related to muscle forces), or (2) the model's performance is superior to the Cartesian force model because of its additional free parameters, and any other "reasonable" model with the same number of additional free parameters would perform about

as well. No definitive conclusion can be drawn on the basis of the current study.

Model Shortcomings

While the model explains much of the response property variation that occurs within single cells, significant residuals remain. The lack of full correspondence between data and model may arise because our fundamental assumption—that M1 represents *only* the biomechanics of movement—is, by necessity, an oversimplification. Rather, it is quite possible that (1) no single representation or even family of representations may adequately capture the response of all M1 neurons (Wu and Hatsopoulos, 2006); (2) motor cortex may be engaged in encoding aspects of movements besides biomechanics (Hoehnerman and Wise, 1991; Ashe and Georgopoulos, 1994); and (3) motor cortex may represent elements of movement in a highly adaptive, nonstationary manner (Wise et al., 1998).

Isometric Tasks versus Movement Tasks in Single-Cell Analyses

An isometric task is defined as the controlled exertion of force by an agent while locked in positional equilibrium with the environment. The ability to perform these tasks comprises only a small subcompetence of biological motor control, the primary purpose of which is movement, i.e., to put the body and its end-effectors in motion for purposes of locomoting, eating, exploring, fighting, etc. It is not surprising, then, that only a handful of studies have examined the neural correlates of whole-arm isometric behavior in motor cortex (Georgopoulos et al., 1992; Taira et al., 1996; Sergio and Kalaska, 1997, 2003; Bolin and Ashe, 2005; Sergio et al., 2005) compared with the many methodologically similar studies that have looked at active movement behavior.

Although movement tasks occur with greater frequency than isometric tasks in naturally behaving animals, this report emphasizes the extraordinary practical advantages of isometric tasks in exploring the neural bases of motor behavior. These advantages include: (1) simplifying the computations of variables involved in force/torque generation; (2) obviating the need for a temporal lag when correlating neural activity with a movement variable; (3) improving upon the signal-to-noise ratio of the correlation due to the constancy of task variables, and (4) reducing the confound of feedback from the periphery. It is these advantages, we believe, that make possible single-cell analyses in the case of isometric tasks, while it would not be possible (given the current state of the field) to conduct similar analyses for a movement task.

While these advantages exist for studying cell response in isometric tasks, it is also possible that two different neural circuits are employed for isometric behavior and movement behavior. Few studies have looked at this issue, and the results of the existing studies are mixed (Sergio et al., 2005; Kurtzer et al., 2005).

Other Means for Single-Cell Analyses

The main point of this paper is that analyses of motor cortical function through single-cell recording studies should, when possible, be performed at the single-cell level to enhance their rigor. We provided one method for assigning model parameters to individual cells based on a multiplicity of task conditions and the use of an isometric task (which enables a virtual equivalence between

muscle force and joint torque reference frames). However, there are many other possibilities involving anatomical methods, physiological methods, or a combination of the two. One idea would be to identify a cell by its cortical connectivity pattern to different muscles, as revealed through anatomical methods, and then to map this connectivity pattern to the parameters of a muscle model. Another possibility would be to identify the downstream muscle targets of a cell through techniques such as spike-triggered averaging (Cheney and Fetz, 1980, 1985; Fetz and Cheney, 1980; Bennett and Lemon, 1996; McKiernan et al., 2000; Park et al., 2004) and then map that muscle field to model parameters.

While this paper supports the viewpoint that the activity of M1 neurons largely reflects the kinetic requirements of motor behavior, other studies have hypothesized that neurons in motor cortex are encoding kinematic parameters of the hand, such as hand position, hand velocity, or hand acceleration (Ashe and Georgopoulos, 1994; Moran and Schwartz, 1999). These hypotheses are easier to test at the single-cell level because of the relative ease with which behavioral variables related to hand kinematics can be accurately measured. For example, suppose that a hand-velocity encoding model fits a neuron's response profile well in one task. Then, if the neuron truly encodes velocity, that same model should apply equally well in explaining response variation in a different task. If neural activity correlates best with hand velocity in one task and with hand acceleration in a different task—or if its tuning parameters otherwise change in a task-dependent fashion—then the observed correlation is likely artifactual.

A Different Functional Interpretation for Gain Variation

Variations in gain have been found in numerous cortical areas subserving a variety of cognitive, sensory, and motor functions (Salinas and Thier, 2000). The classical functional interpretation of these gain variations postulates a multiplexing of distinct sources of information for the purpose of effecting a computation. This interpretation originally arose out of the work of Richard Andersen and colleagues on the representation of saccadic eye movements in posterior parietal cortex (PPC) (Andersen and Mountcastle, 1983; Andersen et al., 1985). According to their findings, neurons in PPC are selectively tuned to a fixed target position in retinotopic coordinates, while the depth of tuning is monotonically modulated by eye position. These two sources of information—retinotopic target position and eye position—can be combined to generate a head-centered representation of the target position in space (Grossberg and Kuperstein, 1986; Zipser and Andersen, 1988; Salinas and Abbott, 1995). This concept of a planar “gain field” computational mechanism for coordinate transformations has since been extended to other types of representation in different cortical regions (Brotchie et al., 1995; Snyder et al., 1998; Kakei et al., 2001; Pesaran et al., 2006).

In contrast, the gain changes in M1 captured by the present single-neuron model do not necessarily represent a computational mechanism by which M1 affects a coordinate transformation. Rather, they are more likely to be an end result of the computations (Ajemian et al., 2001) by which M1 transforms inputs about arm posture and the desired extrinsic spatial direction of static force output at the hand into an output signal about the intrinsic (joint- or muscle-centered) spatial kinetics of motor output.

Peter Strick and colleagues have investigated response property differences of wrist-related cells in both M1 and the ventral premotor area (PMv) (Kakei et al., 1999, 2001, 2003). They found that cells in M1 tended to show sizeable shifts in preferred direction, similar to muscles, while cells in PMv exhibited spatially invariant preferred directions. This would suggest that the representation of movement in PMv maintains a strong spatial character as compared with M1, where the conversion into motor output is more nearly complete. This functional differentiation between the two areas is also strikingly demonstrated by Cisek et al. (2003), who showed that many PMd cells are strongly directionally tuned during the delay period before reaching movements of either the contralateral or ipsilateral arm, with similar extrinsic spatially preferred directions with either arm. In contrast, most M1 neurons, like proximal-arm muscles, were largely activated only by movements of the contralateral arm, and any activity during ipsilateral arm movements usually had very different directional tuning. In light of the above discussion on alternative functional interpretations of gain changes, it would be interesting to see whether the patterns of gain changes in the two areas reflect such a functional dichotomy as well.

EXPERIMENTAL PROCEDURES

Behavioral Task

Juvenile male rhesus monkeys were trained to exert isometric forces with their whole arm by grabbing a manipulandum that was attached to a six-DOF force transducer and clamped to a workspace location. The force level recorded by the transducer controlled the position of a cursor on a computer monitor, such that the x and y components of the force vector (where the xy plane is horizontal) were mapped to a corresponding point on the plane of the video screen. There were eight targets spaced uniformly along the periphery of a circle, each of magnitude 1.5 N. When a target appeared, the monkey generated a 1.5 N force ramp in the appropriate direction, without generating excess force in the vertical direction. When the cursor reached the target, the monkey maintained the position of the cursor—i.e., maintained the 1.5 N force level—for 2000 ms. All data in this paper are taken from this 2000 ms target-hold epoch. Each of the eight target directions was presented five times in a pseudorandom fashion.

Data in this paper are taken from recordings of two monkeys: 42 neurons were recorded from the first monkey, and 12 neurons, from the second. The manipulandum was clamped at nine different workspace locations (see Figure 1) contained within a transverse plane slightly below shoulder level. For the first animal, the spatial positions of the limb joints were also recorded with optical sensors during one daily session, and the corresponding joint angles were imputed through standard reconstruction techniques. For the second animal, the postures measured with the first animal were assumed to apply. To the extent this assumption is incorrect, there will be error introduced into the analyses and, indeed, the single-cell fits were slightly better for the first monkey. However, we felt this was a reasonable approximation for three reasons: (1) the distance between the animal's shoulder and the manipulandum apparatus was the same in both cases; (2) the absolute arm lengths and relative arm proportions were similar; and (3) the animals appeared to assume similar postures from visual inspection. As there was no statistically significant difference in the single-cell fits across the two animals, this assumption may be justified. For further details on the apparatus, task behavior, or data collection methods, see Sergio and Kalaska (2003).

Computational Model

To simulate cell activity according to Equation 2, the transpose Jacobian of the kinematic equations must be computed. The following four-DOF arm model was used:

$$\begin{bmatrix} x \\ y \\ z \end{bmatrix} = \begin{bmatrix} k_2 \cos \theta_1 \cos \theta_3 \sin \varphi + k_2 \sin \theta_1 \sin \theta_2 \sin \theta_3 \sin \varphi + k_2 \sin \theta_1 \cos \theta_2 \cos \varphi + k_1 \sin \theta_1 \cos \theta_2 \\ k_2 \cos \theta_2 \sin \theta_3 \sin \varphi - k_2 \sin \theta_2 \cos \varphi - k_1 \sin \theta_2 \\ -k_2 \sin \theta_1 \cos \theta_3 \sin \varphi + k_2 \cos \theta_1 \sin \theta_2 \sin \theta_3 \sin \varphi + k_2 \cos \theta_1 \cos \theta_2 \cos \varphi + k_1 \cos \theta_1 \cos \theta_2 \end{bmatrix} \quad (7)$$

where θ_1 is the angle of shoulder flexion/extension, θ_2 is the angle of shoulder adduction/abduction, θ_3 is the angle of internal/external rotation of the shoulder, φ is the elbow angle, and the order of shoulder rotation proceeds from θ_1 to θ_3 . The coordinates x , y , and z signify a Cartesian coordinate system centered at the shoulder with the x axis aligned in the ventral-dorsal direction, the y axis aligned in the medial-distal direction, and the z axis aligned in the cranial-caudal direction. k_1 and k_2 are the upper and lower limb lengths, respectively.

Because of motor redundancy, Equation 3 does not uniquely specify the applied joint torques. There exists a 2D null space of joint torques that add no net force at the hand, because their effect is to either cancel at the hand or to induce strain on the joints/connective tissue. Torque vectors from this null space could be arbitrarily added to a vector in the solution space to create another viable torque vector. We take the Moore-Penrose pseudoinverse, which implies that the joint torque contribution from the null space is 0 (i.e., a minimum torque solution). For a well-rehearsed motor task, one might expect that torques would not be produced if their purpose were simply to cancel at the hand or add strain to the system. EMG recordings from both of the highly over-trained monkeys showed strong reciprocal activation of antagonist muscles during the stable isometric equilibria, with minimal coactivation (Sergio and Kalaska, 1997, 2003), further validating this assumption.

Equation 2 postulates a linear relationship between joint torques and cell activity. At some point when the joint torques reach a high enough level, linearity can no longer be maintained because neural activity will saturate. If the arm is not near a singular posture, this saturation occurs when the linearity between muscle activation and muscle force output breaks down. At submaximal muscle force levels, muscle activation is linearly related to muscle activity (Zajac, 1989). The level of end-effector forces in this experiment is 1.5 N., a level significantly below the maximal level of force exertion for the species *Macaca mulatta* (Graham and Scott, 2003). Nevertheless, saturation of M1 activity at intermediate force output levels has been observed (Evarts et al., 1983; Kalaska et al., 1989), and such saturation could contribute to some of the inability of the single-neuron model to predict PD changes and, especially, gain changes at different postures.

Data Analysis

Standard tuning curves in the form of Equation 1 were computed for each cell at each posture on the basis of the average firing rate across the target-hold epoch. However, not all of these tuning curves are necessarily statistically significant. To ensure that response tuning was unlikely to have occurred by chance, a bootstrapping procedure (Georgopoulos et al., 1988; Scott and Kalaska, 1997; Sergio and Kalaska, 2003) was used to assess the statistical significance of each tuning curve. Of the 42 cells from the first animal, 39 showed statistically significant tuning curves at all nine postures. For one cell, statistically significant tuning curves were found at eight postures. For another cell, the number of postures was seven. And for the final cell, the number of postures was six. In all cases, the tuning curve was well defined at the central posture. These 42 cells, together with 12 cells from the second animal, with tuning curves computed at all postures, constitute the complete data set for both the population and single-cell analyses.

The analyses were run both including and excluding data from the six postures across three cells where tuning curves were not well defined. The results were virtually identical. The reported figures exclude these six instances (because these tuning curves are not well defined), meaning that for the single-cell analyses, there are 426 (i.e., $54 \times 8 - 6$) instances of cell gain and 480 (i.e., $54 \times 9 - 6$) instances of cell PD measures.

Two methods were used to establish single-cell fits to the data. In the first method, two free model parameters were used to precisely fit the cell's PD at the central posture. With the remaining free parameter, the eight gain change values per cell were fit using the least mean squares (LMS) criterion

on the fractional gain changes—that is, the model parameter was adjusted until the LMS error of the real fractional gain changes with the model fractional changes reached its minimum. The nonlinear optimization algorithm was run several times to ensure stable convergence. It is critical to note that the free model parameters were not simply components of $\vec{\tau}_{PD}$ along one of the axes in joint torque space (i.e., the shoulder flexion component). Rather, the free parameters were simply individual points in the 4D joint torque space that were, in general, a linear combination of the basis vectors (a parameter is some combination of all four joint torque components). Standard linear correlation was used to determine the goodness of fit of the model gain changes to the actual gain changes.

In the second method, all three free model parameters were used to fit the eight gain change values per cell according to the same LMS criterion. No parameters were devoted to the PDs. In determining the goodness of fit of the model PDs to the actual PDs, circular statistics were used (Fisher, 1993). First, a circular correlation coefficient was computed using the T-linear association model. The null hypothesis of zero correlation was rejected. Second, a bootstrap method was used. The histogram of differences between actual and predicted PD values was compared with a histogram of bootstrapped samples of differences, which was constructed by sampling two PDs randomly (with replacement) from the data.

To assess the significance of the correlation between the preferred torque vectors computed by the two different methods, a bootstrapping analysis was used. Pairs of 4D vectors were randomly generated by sampling each component from a uniform distribution on the interval $[-1, 1]$. These vectors were subsequently normalized and their dot product was taken.

These simulations were extremely robust across parameter variations. For details of the sensitivity analyses at both the population level and the single-cell level, see [Supplementary Material](#).

APPENDIX A

Muscle Force Encoding

Here we show that if the matrix of moment arms varies across the workspace slowly in comparison to the Jacobian, then the results on PD shifts and gain changes hold whether the recruitment rule utilizes a dot product of joint torques or muscle forces. In the [Supplementary Material](#), we actually calculate the different rates of change of the two matrices and show quantitatively in the case of a two-DOF arm that the matrix of moment arms varies slowly compared with the Jacobian.

Suppose cells are activated according to Equation 2. Then a cell's preferred direction, ω_{PD} , as determined by an experimenter at arm posture θ_k , can be written as

$$\omega_{PD} = \omega_i: \max\{\vec{\tau}_{PD}^T \mathbf{J}^T(\theta_k) \vec{F}_i\} \quad (A1)$$

$$\omega_{PD} = \omega_i: \max\{\vec{\tau}_{PD}^T \mathbf{J}^T(\theta_k) \|F\| \begin{pmatrix} \cos \omega_i \\ \sin \omega_i \end{pmatrix}\} \quad (A2)$$

where $\|F\|$ is the magnitude of the force vector used in a center-out isometric task, and ω_i is the angle of exertion. Note how the dot product has been replaced by vector multiplication using the transpose operation. If instead cells are activated according to Equation 4, and if the matrix of moment arms can be inverted as in Equation 6, then a cell's preferred direction can be written as

$$\omega_{PD} = \omega_i: \max\{\vec{\mathbf{M}}_{PD}^T \mathbf{J}_M^T(\theta_k)^{-1} \mathbf{J}^T(\theta_k) \|F\| \begin{pmatrix} \cos \omega_i \\ \sin \omega_i \end{pmatrix}\}. \quad (A3)$$

For the sake of simplicity, assume that the set of muscles can be divided into agonist/antagonist pairs that act about the same joint (or joints in the case of

biarticular muscles). In this way, a negative component of the muscle force vector indicates that the antagonist force exceeds the agonist force.

A preferred muscle force vector, $\vec{\mathbf{M}}_{PD}$, can exist anywhere in the high-dimensional muscle space. However, only those vector components that project into the space of actually utilized muscle forces contribute to cell activity. Since a specific inversion of the matrix of moment arms has been assumed, the space of actually utilized muscle forces is the 4D image space of $\mathbf{J}_M^T(\theta_k)^{-1}$. Note that this does not mean that only four muscle pairs are used during force generation; rather, it means that the criterion used to resolve redundancy leads to a 4D muscle force space, where a basis vector can be a high-dimensional combination or “synergy” of muscle forces. Therefore, the preferred muscle force vectors can, through projection onto this space and subsequent conversion into torque space, be written as $\mathbf{J}_M^T(\theta_k)^{-1} \vec{\tau}_{PD}$, leading to

$$\omega_{PD} = \omega_i: \max\left\{\left(\mathbf{J}_M^T(\theta_k)^{-1} \vec{\tau}_{PD}\right)^T \left(\mathbf{J}_M(\theta_k)^{-1}\right)^T \mathbf{J}^T(\theta_k) \|F\| \begin{pmatrix} \cos \omega_i \\ \sin \omega_i \end{pmatrix}\right\} \quad (A4)$$

where the distribution of $\vec{\tau}_{PD}$ is uniform if the distribution of $\vec{\mathbf{M}}_{PD}$ is uniform (i.e., directions are being mapped to directions). Rewriting yields

$$\omega_{PD} = \omega_i: \max\left\{\vec{\tau}_{PD}^T \mathbf{J}_M(\theta_k)^{-1} \left(\mathbf{J}_M(\theta_k)^{-1}\right)^T \mathbf{J}^T(\theta_k) \|F\| \begin{pmatrix} \cos \omega_i \\ \sin \omega_i \end{pmatrix}\right\}. \quad (A5)$$

Although moment arms are posture dependent, both experimental and modeling studies in humans indicate that moment arms remain relatively constant across “small” regions of the workspace (Amis et al., 1979; An et al., 1981; Winters and Kleweno, 1993; Murray et al., 1995). For example, Murray et al. (1995) demonstrated through measurements and computer simulation that elbow flexors/extensors vary about 30% over a 95° range. In comparison, the components of the Jacobian matrix will change sign over the same angular range. The only study that rigorously investigated the variation of moment arms in nonhuman primates is Graham and Scott (2003). Overall, they found similarly moderate variations in moment arms for 14 muscles spanning the elbow and shoulder in the species *M. mulatta*, which is the same species employed in the isometric task of Drs. Sergio and Kalaska. In the [Supplementary Data](#), we use the data of Graham and Scott (2003) to compute variation in the matrix of moment arms in a circular region of space for a two-DOF arm. We compare this variation to the variation in the Jacobian and show that the variation in the Jacobian is much greater.

Therefore, we consider $\mathbf{J}_M^T(\theta_k)$ to be constant relative to $\mathbf{J}^T(\theta_k)$, and we can make the approximation that $(\forall i, j) : i, j = 1 \dots 9 \mathbf{J}_M(\theta_{k_i}) \approx \mathbf{J}_M(\theta_{k_j})$. With this approximation,

$$\omega_{PD} = \omega_i: \max\left\{\vec{\tau}_{PD}^T \mathbf{S} \mathbf{J}^T(\theta_k) \|F\| \begin{pmatrix} \cos \omega_i \\ \sin \omega_i \end{pmatrix}\right\} \quad (A6)$$

where $\mathbf{S} = \mathbf{J}_M(\theta)^{-1} (\mathbf{J}_M(\theta)^{-1})^T$ remains constant across postures. As the product of a matrix and its transpose, \mathbf{S} is a positive semidefinite matrix; further, since the matrix of moment arms has more rows than columns (there are more muscles than joint DOFs), \mathbf{S} is strictly positive definite. The transpose of a positive definite matrix is itself, so Equation A6 can be rewritten as

$$\omega_{PD} = \omega_i: \max\left\{(\mathbf{S} \vec{\tau}_{PD})^T \mathbf{J}^T(\theta_k) \|F\| \begin{pmatrix} \cos \omega_i \\ \sin \omega_i \end{pmatrix}\right\}. \quad (A7)$$

Note that in this expression, only $\mathbf{J}^T(\theta_k)$ varies with posture, and thus it alone determines the PD shifts and gain changes. The expression $(\mathbf{S} \vec{\tau}_{PD})^T$ indicates that the assumption of muscle force coding with a uniform distribution of preferred muscle force vectors reduces to the case of joint torque coding, with a nonuniform distribution of preferred joint torque vectors as determined by the effect of the transformation \mathbf{S} . As indicated in the text, altering the distribution of preferred joint torque vectors does not materially change the results on PD shifts and gain changes, as long as \mathbf{S} is not singular (or near singular). Because \mathbf{S} is positive definite (and not merely positive semidefinite), it is guaranteed to be nonsingular.

Muscle Activation Encoding

In an isometric task, the relationship between muscle activation and muscle force can be written as follows (Zajac, 1989):

$$\mathbf{M}_i = \lambda_i \mathbf{E}_i f_i f_v \quad (A8)$$

where \mathbf{M}_i is the force exerted by the i^{th} muscle, \mathbf{E}_i is activation of the i^{th} muscle, f_i is a normalized force-length curve, f_v is a normalized force-velocity curve, and λ_i is a muscle-specific scale factor that does not depend on muscle state. In an isometric task, the muscle shortening velocity is 0 and the muscle length is held constant. The former implies that $f_v = 1$ and so can be eliminated; the latter implies that f_i is constant at a given posture across all force directions,

Table A1. Preferred Torque Vectors as Computed with the Two Different Methods

	Method 1				Method 2				C
	$\delta\theta_1$	$\delta\theta_2$	$\delta\theta_3$	$\delta\varphi$	$\delta\theta_1$	$\delta\theta_2$	$\delta\theta_3$	$\delta\varphi$	
Cell 1	0.58	0.34	-0.57	-0.47	0.63	0.35	-0.52	-0.47	0.99
Cell 2	0.14	0.87	-0.44	-0.15	-0.53	0.79	-0.19	-0.22	0.73
Cell 3	-0.59	0.02	0.09	0.80	-0.55	0.17	0.32	0.75	0.96
Cell 4	0.28	0.31	0.74	0.53	-0.08	0.14	0.77	0.62	0.92
Cell 5	-0.08	0.75	-0.64	-0.13	-0.44	0.44	-0.75	0.23	0.82
Cell 6	-0.55	-0.16	0.81	0.12	-0.97	0.02	0.22	0.07	0.72
Cell 7	-0.55	-0.28	0.78	0.05	-0.51	-0.28	0.81	0.05	0.99
Cell 8	-0.52	-0.56	0.50	0.42	0.54	-0.37	0.44	0.61	0.40
Cell 9	0.48	0.75	-0.06	-0.46	-0.48	0.71	-0.18	-0.49	0.54
Cell 10	-0.60	0.03	0.79	0.15	-0.58	0.04	0.80	0.13	0.99
Cell 11	0.43	0.58	-0.04	-0.69	0.20	0.72	-0.21	-0.64	0.95
Cell 12	0.16	0.49	0.29	0.81	-0.30	0.66	0.68	0.06	0.52
Cell 13	0.43	0.02	0.67	0.61	-0.13	-0.11	-0.04	0.98	0.51
Cell 14	-0.70	-0.10	0.68	-0.17	-0.87	-0.06	0.45	-0.19	0.95
Cell 15	-0.29	-0.18	0.42	-0.84	-0.35	-0.24	0.23	-0.87	0.97
Cell 16	0.23	-0.25	-0.04	0.94	0.23	-0.25	-0.03	0.94	0.99
Cell 17	-0.09	-0.93	-0.35	0.06	-0.09	-0.70	-0.38	-0.60	0.76

(Continued on next page)

Table A1. Continued

	Method 1				Method 2				C
	$\delta\theta_1$	$\delta\theta_2$	$\delta\theta_3$	$\delta\phi$	$\delta\theta_1$	$\delta\theta_2$	$\delta\theta_3$	$\delta\phi$	
Cell 18	0.56	0.70	-0.03	-0.45	0.61	0.67	0.15	-0.41	0.99
Cell 19	0.32	0.29	-0.69	-0.59	-0.47	0.28	-0.51	-0.66	0.67
Cell 20	0.32	-0.66	0.41	-0.54	0.37	-0.78	0.30	-0.40	0.97
Cell 21	-0.29	0.31	0.85	-0.32	-0.56	0.43	0.71	0.09	0.87
Cell 22	-0.21	0.21	0.95	0.02	-0.56	0.22	0.41	0.69	0.57
Cell 23	0.63	0.65	0.06	-0.42	-0.06	0.92	-0.32	0.24	0.44
Cell 24	-0.05	0.65	0.25	0.72	-0.28	0.84	0.25	0.39	0.90
Cell 25	0.05	0.59	-0.80	-0.05	0.41	0.55	-0.73	-0.07	0.93
Cell 26	0.23	-0.54	0.74	0.33	-0.58	-0.39	0.56	0.44	0.64
Cell 27	-0.50	0.84	-0.04	0.20	0.26	0.83	0.09	0.48	0.66
Cell 28	0.49	-0.37	0.74	-0.28	0.89	-0.36	-0.07	0.26	0.44
Cell 29	-0.33	0.59	0.65	0.35	0.25	0.60	0.52	-0.55	0.42
Cell 30	-0.33	0.06	0.89	-0.30	-0.73	0.16	0.38	0.55	0.42
Cell 31	-0.44	-0.44	-0.30	0.72	-0.07	-0.40	-0.91	-0.12	0.39
Cell 32	-0.17	-0.46	-0.39	0.78	0.20	-0.60	-0.72	0.28	0.74
Cell 33	0.81	-0.53	-0.24	0.01	0.09	0.85	-0.17	0.49	-0.33
Cell 34	0.57	-0.55	-0.40	0.46	0.16	-0.91	-0.18	0.33	0.82
Cell 35	-0.20	0.39	0.89	-0.13	-0.33	0.36	0.87	-0.04	0.99
Cell 36	-0.13	0.66	0.15	0.73	-0.54	0.68	0.37	0.34	0.82
Cell 37	0.52	0.15	-0.74	-0.40	0.19	0.01	-0.88	-0.44	0.93
Cell 38	-0.33	0.39	0.86	0.01	-0.47	0.41	0.77	0.12	0.98
Cell 39	0.35	-0.12	-0.36	0.86	0.25	0.13	0.27	-0.92	-0.82
Cell 40	-0.01	-0.84	0.35	-0.42	0.36	-0.39	-0.28	0.80	-0.11
Cell 41	-0.54	-0.24	0.18	-0.79	-0.50	-0.44	0.23	-0.71	0.98
Cell 42	-0.35	-0.36	-0.23	-0.83	0.19	-0.65	-0.74	0.06	0.29
Cell 43	0.35	-0.43	-0.73	-0.40	0.17	-0.57	-0.80	-0.14	0.94
Cell 44	-0.05	-0.56	-0.81	0.19	0.38	-0.48	-0.69	-0.38	0.74
Cell 45	0.62	-0.18	-0.34	-0.68	0.57	-0.05	-0.15	-0.81	0.96
Cell 46	0.03	0.77	-0.07	0.62	0.08	0.23	0.04	0.97	0.78
Cell 47	-0.32	0.15	0.92	-0.16	-0.34	0.14	0.92	-0.14	0.99
Cell 48	-0.05	0.62	-0.10	0.78	0.04	0.60	-0.06	0.80	0.99
Cell 49	0.86	-0.20	-0.47	-0.02	0.50	-0.16	-0.78	0.33	0.82
Cell 50	-0.53	0.05	0.19	0.83	-0.48	0.12	0.28	0.82	0.99
Cell 51	0.33	-0.16	-0.46	-0.81	0.39	-0.10	-0.32	-0.86	0.99
Cell 52	0.08	0.77	0.36	0.52	0.37	-0.56	-0.34	0.66	-0.18
Cell 53	-0.42	-0.09	0.23	0.87	0.07	0.23	0.54	0.81	0.78
Cell 54	-0.47	0.43	0.16	0.75	-0.18	0.52	-0.05	0.83	0.92

In Method 1, two free parameters were used to fit the preferred direction at the center location, and the remaining free parameter was used to fit the peripheral gains. In Method 2, all three free parameters were used to fit the peripheral gains. Details are in the [Experimental Procedures](#). The correlation between these measures was assessed using a dot product. The first 42 cells are from the first animal.

and so will end up being incorporated into b_0 , the baseline level of cell activity. As a result of these simplifications, muscle force can be related to muscle activation via a diagonal matrix, and this relationship can be inverted. Thus, the arguments of the previous subsection (Muscle Force Encoding) can be extended to the case of muscle activation coding.

SUPPLEMENTAL DATA

The Supplemental Data for this article can be found online at <http://www.neuron.org/cgi/content/full/58/3/414/DC1/>.

ACKNOWLEDGMENTS

We thank Emilio Bizzi, Paul Cisek, Neville Hogan, and three anonymous reviewers for their insightful comments. R.A. was funded by the Charles A. King Trust (Bank of America, Co-trustee) Fellowship and by the McGovern Institute for Brain Research. A.G. was supported by an NIH grant (NIH R01-NS046033), a CIHR Net Grant (NET-54000), and a CIHR postdoctoral fellowship. L.S. and J.K. were supported by operating grants from the CIHR, and J.K. was also supported by an infrastructure grant from the FRSQ. D.B. and S.G. were supported in part by NSF Grant SBE-0354378.

Received: February 19, 2007

Revised: July 13, 2007

Accepted: February 12, 2008

Published: May 7, 2008

REFERENCES

- Ajemian, R., Bullock, D., and Grossberg, S. (2000). Kinematic coordinates in which motor cortical cells encode movement direction. *J. Neurophysiol.* *84*, 2191–2203.
- Ajemian, R., Bullock, D., and Grossberg, S. (2001). A model of movement coordinates in the motor cortex: posture-dependent changes in the gain and direction of single cell tuning curves. *Cereb. Cortex* *11*, 1124–1135.
- Amis, A.A., Dowson, D., and Wright, V. (1979). Muscle strengths and musculo-skeletal geometry of the upper limb. *Eng. Med.* *8*, 41–47.
- An, K.N., Hui, F.C., Moreey, B.F., Linscheid, R.L., and Chao, E.Y. (1981). Muscles across the elbow joint: a biomechanical analysis. *J. Biomech.* *14*, 659–669.
- Andersen, R.A., and Mountcastle, V.B. (1983). The influence of the angle of gaze upon the excitability of the light-sensitive neurons of the posterior parietal cortex. *J. Neurosci.* *3*, 532–548.
- Andersen, R.A., Essick, G.K., and Siegel, R.M. (1985). Encoding of spatial location by posterior parietal neurons. *Science* *230*, 456–458.
- Ashe, J., and Georgopoulos, A.P. (1994). Movement parameters and neural activity in motor cortex and area 5. *Cereb. Cortex* *4*, 590–600.
- Baraduc, P., Guigon, E., and Burnod, Y. (2001). Recoding arm position to learn visuomotor transformations. *Cereb. Cortex* *11*, 906–917.
- Bennett, K.M., and Lemon, R.N. (1996). Corticomotoneuronal contribution to the fractionation of muscle activity during precision grip in the monkey. *J. Neurophysiol.* *75*, 1826–1842.
- Boline, J., and Ashe, J. (2005). On the relations between single cell activity in the motor cortex and the direction and magnitude of three-dimensional dynamic isometric force. *Exp. Brain Res.* *167*, 148–159.
- Brotchie, P.R., Andersen, R.A., Snyder, L.H., and Goodman, S.J. (1995). Head position signals used by parietal neurons to encode locations of visual stimuli. *Nature* *375*, 232–235.
- Bullock, D., and Grossberg, S. (1988). Neural dynamics of planned arm movements: emergent invariants and speed-accuracy properties during trajectory formation. *Psychol. Rev.* *95*, 49–90.
- Bullock, D., Cisek, P., and Grossberg, S. (1998). Cortical networks for control of voluntary arm movements under variable force conditions. *Cereb. Cortex* *8*, 48–62.
- Cabel, D.W., Cisek, P., and Scott, S.H. (2001). Neural activity in primary motor cortex related to mechanical loads applied to the shoulder and elbow during a postural task. *J. Neurophysiol.* *86*, 2102–2108.
- Caminiti, R., Johnson, P.B., and Urbano, A. (1990). Making arm movements within different parts of space: Dynamic aspects in the primate motor cortex. *J. Neurosci.* *10*, 2039–2058.
- Cheney, P.D., and Fetz, E.E. (1980). Functional classes of primate corticomotoneuronal cells and their relation to active force. *J. Neurophysiol.* *44*, 773–791.
- Cheney, P.D., and Fetz, E.E. (1985). Comparable patterns of muscle facilitation evoked by individual corticomotoneuronal (CM) cells and by single intracortical microstimuli in primates: evidence for functional groups of CM cells. *J. Neurophysiol.* *53*, 786–804.
- Cisek, P., and Kalaska, J.F. (2005). Neural correlates of reaching decisions in dorsal premotor cortex: specification of multiple direction choices and final selection of action. *Neuron* *45*, 801–814.
- Cisek, P., Crammond, D.J., and Kalaska, J.F. (2003). Neural activity in primary motor and dorsal premotor cortex in reaching tasks with the contralateral versus ipsilateral arm. *J. Neurophysiol.* *89*, 922–942.
- Crammond, D.J., and Kalaska, J.F. (1996). Differential relation of discharge in primary motor cortex and premotor cortex to movements versus actively maintained postures during a reaching task. *Exp. Brain Res.* *108*, 45–61.
- Crammond, D.J., and Kalaska, J.F. (2000). Prior information in motor and premotor cortex: activity during the delay period and effect on pre-movement activity. *J. Neurophysiol.* *84*, 986–1005.
- Evarts, E.V. (1968). Relation of pyramidal tract activity to force exerted during voluntary movement. *J. Neurophysiol.* *31*, 14–27.
- Evarts, E.V. (1969). Activity of pyramidal tract neurons during postural fixation. *J. Neurophysiol.* *32*, 375–385.
- Evarts, E.V., Fromm, C., Kroller, J., and Jennings, V.A. (1983). Motor Cortex control of finely graded forces. *J. Neurophysiol.* *49*, 1199–1215.
- Ferrier, D. (1873). Experimental researches in cerebral physiology and pathology. *West Riding Lunatic Asylum Medical Reports* *3*, 30–96.
- Fetz, E.E., and Cheney, P.D. (1980). Postspike facilitation of forelimb muscle activity by primate corticomotoneuronal cell. *J. Neurophysiol.* *44*, 751–772.
- Fetz, E.E., Cheney, P.D., Mewes, K., and Palmer, S. (1989). Control of forelimb muscle activity by populations of corticomotoneuronal and rubromotoneuronal cells. In *Progress in Brain Research: Afferent Control of Posture and Locomotion*, J.H.J. Allum and M. Hulliger, eds. (Amsterdam: Elsevier Science), pp. 437–449.
- Fisher, N.I. (1993). *Statistical Analysis of circular data* (Cambridge: Cambridge University Press).
- Fritsch, G.T., and Hitzig, E. (1870). Über die elektrische Erregbarkeit des Grosshirns. *Arch. Anat. Physiol. Med. Wiss.* *300*, 32.
- Gandolfo, F., Li, C.S., Benda, B.J., Padoa-Schioppa, C., and Bizzi, E. (2000). Cortical correlates of learning in monkeys adapting to a new dynamical environment. *Proc. Natl. Acad. Sci. USA* *97*, 2259–2263.
- Georgopoulos, A.P. (1995). Current issues in directional motor control. *Trends Neurosci.* *18*, 506–510.
- Georgopoulos, A.P., Kalaska, J.F., Caminiti, R., and Massey, J.T. (1982). On the relations between the direction of two-dimensional arm movements and cell discharge in primate motor cortex. *J. Neurosci.* *2*, 1527–1537.
- Georgopoulos, A.P., Caminiti, R., and Kalaska, J.F. (1984). Static spatial effects in motor cortex and area 5: Quantitative Relations in a two-dimensional space. *Exp. Brain Res.* *54*, 446–454.
- Georgopoulos, A.P., Kettner, R.E., and Schwartz, A.B. (1988). Primate motor cortex and free arm movements to visual targets in three-dimensional space. II. Coding of the direction of movement by a neuronal population. *J. Neurosci.* *8*, 2928–2937.
- Georgopoulos, A.P., Ashe, J., Smyrnis, N., and Taira, M. (1992). The motor cortex and the coding of force. *Science* *256*, 1692–1695.
- Graham, K.M., and Scott, S.H. (2003). Morphometry of Macaca mulatta forelimb. III. Moment arm of shoulder and elbow muscles. *J. Morphol.* *255*, 301–314.
- Gribble, P.L., and Scott, S.H. (2002). Overlap of internal models in motor cortex for mechanical loads during reaching. *Nature* *417*, 938–941.
- Grossberg, S., and Kuperstein, M. (1986). *Neural dynamics of adaptive sensory-motor control* (New York: Elsevier Science).
- Herter, T.M., Kurtzer, I., Cabel, D.W., Haunts, K.A., and Scott, S.H. (2007). Characterization of torque-related activity in primary motor cortex during a multijoint postural task. *J. Neurophysiol.* *97*, 2887–2899.
- Hocherman, S., and Wise, S.P. (1991). Effects of hand movement path on motor cortical activity in awake, behaving rhesus monkeys. *Exp. Brain Res.* *83*, 285–302.
- Takei, S., Hoffman, D.S., and Strick, P.L. (1999). Muscle and movement representations in the primary motor cortex. *Science* *285*, 2136–2139.
- Takei, S., Hoffman, D.S., and Strick, P.L. (2001). Direction of action is represented in the ventral premotor cortex. *Nat. Neurosci.* *4*, 1020–1025.
- Takei, S., Hoffman, D.S., and Strick, P.L. (2003). Sensorimotor transformations in cortical motor areas. *Neurosci. Res.* *46*, 1–10.
- Kalaska, J.F., and Hyde, M.L. (1985). Area 4 and area 5: differences between the load direction-dependent discharge variability of cells during active postural fixation. *Exp. Brain Res.* *59*, 197–202.
- Kalaska, J.F., Cohen, D.A.D., Hyde, M.L., and Prud'homme, M. (1989). A comparison of movement direction-related versus load direction-related activity in primate motor cortex, using a two-dimensional reaching task. *J. Neurosci.* *9*, 2080–2102.

- Kettner, R.E., Schwartz, A.B., and Georgopoulos, A.P. (1988). Primate motor cortex and free arm movements to visual targets in three-dimensional space. III. Positional gradients and population coding of movement direction from various movement origins. *J. Neurosci.* 8, 2938–2947.
- Kurtzer, I., Herter, T.M., and Scott, S.H. (2005). Random change in cortical load representation suggests distinct control of posture and movement. *Nat. Neurosci.* 8, 498–504.
- Lacquaniti, F., Guigon, E., Bianchi, L., Ferraina, S., and Caminiti, R. (1995). Representing spatial information for limb movement: role of area 5 in the monkey. *Cereb. Cortex* 5, 391–409.
- Loeb, G.E., Brown, I.E., and Scott, S.H. (1996). Directional motor control. *Trends Neurosci.* 19, 137–138.
- McKiernan, B.J., Marcario, K.K., Karrer, J.H., and Cheney, P.D. (2000). Correlations between corticomotoneuronal (CM) cell postspike effects and cell-target muscle covariation. *J. Neurophysiol.* 83, 99–115.
- Moran, D.W., and Schwartz, A.B. (1999). Motor cortical representation of speed and direction during reaching. *J. Neurophysiol.* 82, 2676–2692.
- Morrow, M.M., and Miller, L.E. (2003). Prediction of muscle activity by populations of sequentially recorded primary motor cortex neurons. *J. Neurophysiol.* 89, 2279–2288.
- Murray, W.M., Delp, S.L., and Buchanan, T.S. (1995). Variation of muscle moment arms with elbow and forearm position. *J. Biomech.* 28, 513–525.
- Mussa-Ivaldi, F.A. (1988). Do neurons in the motor cortex encode movement direction? An alternate hypothesis. *Neurosci. Lett.* 91, 106–111.
- Padoa-Schioppa, C., Li, C.S., and Bizzi, E. (2001). Neuronal correlates of kinematics-to-dynamics transformation in the supplementary motor area. *Neuron* 36, 751–765.
- Park, M.C., Belhaj-Saif, A., and Cheney, P.D. (2004). Properties of primary motor cortex output to forelimb muscles in rhesus macaques. *J. Neurophysiol.* 92, 2968–2984.
- Pesaran, B., Nelson, M.J., and Andersen, R.A. (2006). Dorsal premotor neurons encode the relative position of the hand, eye, and goal during reach planning. *Neuron* 51, 125–134.
- Phillips, C.G. (1975). Laying the ghost of ‘muscles versus movements.’ *Can. J. Neurol. Sci.* 2, 209–218.
- Rathelot, J.A., and Strick, P.L. (2006). Muscle representation in the macaque motor cortex: an anatomical perspective. *Proc. Natl. Acad. Sci. USA.* 103, 8257–8262.
- Salinas, E., and Abbott, L.F. (1995). Transfer of coded information from sensory to motor networks. *J. Neurosci.* 15, 6461–6474.
- Salinas, E., and Thier, P. (2000). Gain modulation: a major computational principle of the central nervous system. *Neuron* 27, 15–21.
- Sanger, T.D. (1994). Theoretical considerations for the analysis of population coding in motor cortex. *Neural Comput.* 6, 29–37.
- Schwartz, A.B., Kettner, R.E., and Georgopoulos, A.P. (1988). Primate motor cortex and free arm movements to visual targets in 3-d space. I. Relations between single cell discharge and direction of movement. *J. Neurosci.* 8, 2913–2927.
- Scott, S.H. (2000). Reply to ‘One motor cortex, two different views’. *Nat. Neurosci.* 3, 964–965.
- Scott, S.H., and Kalaska, J.F. (1997). Reaching movements with similar hand paths but different arm orientations. I. Activity of individual cells in motor cortex. *J. Neurophysiol.* 77, 826–852.
- Scott, S.H., Gribble, P.L., Graham, K.M., and Cabel, D.W. (2001). Dissociation between hand motion and population vectors from neural activity in motor cortex. *Nature* 413, 161–165.
- Sergio, L.E., and Kalaska, J.F. (1997). Systematic changes in directional tuning of motor cortex cell activity with hand location in the workspace during generation of static isometric forces in constant spatial directions. *J. Neurophysiol.* 78, 1170–1174.
- Sergio, L.E., and Kalaska, J.F. (1998). Changes in the temporal pattern of primary motor cortex activity in a directional isometric force versus limb movement task. *J. Neurophysiol.* 80, 1577–1583.
- Sergio, L.E., and Kalaska, J.F. (2003). Systematic changes in motor cortex cell activity with arm posture during directional isometric force generation. *J. Neurophysiol.* 89, 212–228.
- Sergio, L.E., Hamel-Paquet, C., and Kalaska, J.F. (2005). Motor cortex neural correlates of output kinematics and kinetics during isometric-force and arm-reaching tasks. *J. Neurophysiol.* 94, 2353–2378.
- Serruya, M.D., Hatsopoulos, N.G., Paninski, L., Fellows, M.R., and Donoghue, J.P. (2002). Instant neural control of a movement signal. *Nature* 416, 141–142.
- Snyder, L.H., Grieve, K.L., Brotchie, P., and Andersen, R.A. (1998). Separate body- and world-referenced representations of visual space in parietal cortex. *Nature* 394, 887–891.
- Taira, M., Bolino, J., Smyrnis, N., Georgopoulos, A.P., and Ashe, J. (1996). On the relations between single cell activity in the motor cortex and the direction and magnitude of three-dimensional static isometric force. *Exp. Brain Res.* 109, 367–376.
- Tanaka, S. (1994). Hypothetical joint-related coordinate systems in which populations of motor cortical neurons code direction of voluntary arm movements. *Neurosci. Lett.* 180, 83–86.
- Taylor, C.S., and Gross, C.S. (2003). Twitches versus movements: a story of motor cortex. *Neuroscientist* 9, 332–342.
- Taylor, D.M., Tillery, S.I., and Schwartz, A.B. (2002). Direct cortical control of 3D neuroprosthetic devices. *Science* 296, 1829–1832.
- Thach, W.T. (1978). Correlation of neural discharge with pattern and force of muscular activity, joint position, and direction of intended next movement in motor cortex and cerebellum. *J. Neurophysiol.* 41, 654–676.
- Todorov, E. (2000). Direct cortical control of muscle activation in voluntary arm movements: a model. *Nat. Neurosci.* 3, 391–398.
- Trainor, E., Meir, R., and Karniel, A. (2007). Explaining patterns of neural activity in the primary motor cortex using spinal cord and limb biomechanics models. *J. Neurophysiol.* 97, 3736–3750.
- Wessberg, J., Stambaugh, C.R., Kralik, J.D., Beck, P.D., Laubach, M., Chapin, J.K., Kim, J., Biggs, S.J., Srinivasan, M.A., and Nicolelis, M.A. (2000). Real-time prediction of hand trajectory by ensembles of cortical neurons in primates. *Nature* 408, 361–365.
- Winters, J.M., and Kleweno, D.G. (1993). Effect of initial upper-limb alignment on muscle contributions to isometric strength curves. *J. Biomech.* 26, 143–153.
- Wise, S.P., Moody, S.L., Blomstrom, K.J., and Mitz, A.R. (1998). Changes in motor cortical activity during visuomotor adaptation. *Exp. Brain Res.* 121, 285–299.
- Wu, W., and Hatsopoulos, N. (2006). Evidence against a single coordinate system representation in the motor cortex. *Exp. Brain Res.* 175, 197–210.
- Zajac, F.E. (1989). Muscle and tendon: properties, models, scaling, and application to biomechanics and motor control. *Crit. Rev. Biomed. Eng.* 17, 359–411.
- Zhang, K., and Sejnowski, T.J. (1999). A theory of geometric constraints on neural activity for natural three-dimensional movement. *J. Neurosci.* 19, 3122–3145.
- Zipser, D., and Andersen, R.A. (1988). A back-propagation programmed network that simulates response properties of a subset of posterior parietal neurons. *Nature* 331, 679–684.